J-band spectroscopy of cataclysmic variables

S. P. Littlefair,[1★] V. S. Dhillon,[1] Steve B. Howell[2] and David R. Ciardi[3]

[1]*Department of Physics and Astronomy, University of Sheffield, Sheffield S3 7RH*
[2]*Department of Physics and Astronomy, University of Wyoming, Laramie, WY 82071, USA*
[3]*Department of Astronomy, University of Florida, Gainesville, FL 32611, USA*

ABSTRACT

We present time-resolved, *J*-band (1.025–1.340 μm) infrared spectra of the short-period dwarf novae (DNe) WZ Sge and VY Aqr, and single spectra of the short-period DN EF Peg and the nova-like variable PX And. There is some evidence in the spectra of VY Aqr and EF Peg that we have detected the secondary star, both in the continuum slope and also through the possible presence of spectral features. The spectra of WZ Sge and PX And, on the other hand, show no evidence for the secondary star, with upper limits for its contribution to the *J*-band light of 10 and 20 per cent respectively. The spectral type of the secondary in WZ Sge is constrained to be later than M7.5V. Using skew mapping, we have been able to derive a value for the radial velocity semi-amplitude of the secondary star in VY Aqr of $K_R = 320 \pm 70\,\mathrm{km\,s^{-1}}$, which in conjunction with K_W from Thorstensen & Taylor gives a mass ratio of $q = 0.15 \pm 0.04$.

Key words: stars: individual: WZ Sge – stars: individual: VY Aqr – stars: individual: EF Peg – stars: individual: PX And – novae, cataclysmic variables – infrared: stars.

1 INTRODUCTION

Cataclysmic variables (CVs) are semidetached binary systems in which a white dwarf primary accretes material from a Roche lobe filling secondary. For a thorough review of CVs see Warner (1995). There is a strong motivation to detect the secondary stars in CVs. A detection of the secondary star is desirable for a reliable estimation of the system parameters, which in turn allow one to test theories of CV evolution, (see, e.g., Smith & Dhillon 1998). In addition, the contribution of the secondary to the total flux can be used to give the distance to the CV (see, e.g., Marsh 1990). Detection of the secondary star is of particular interest in CVs below the period gap. The models of Kolb (1993) predict that 99 per cent of the present-day population of CVs should be below the period gap, and that around 70 per cent of these systems will have already reached the orbital period minimum. Modelling of the secondary stars in post-period-minimum CVs has been performed by Howell, Rappaport & Politano (1997), who find them to be degenerate, brown dwarf-like objects with masses between 0.02 and $0.06\,\mathrm{M_\odot}$. Howell et al. (1997) further speculate that the tremendous outburst amplitude dwarf novae (TOADs) are these post-period-minimum CVs. Estimates of the parameters of the secondary stars would provide us with tests for these claims, as well as allowing us to investigate the mass–radius relation of the brown dwarf-like secondary by invoking the Roche lobe filling criterion.

Previous attempts to detect the secondary star in CVs have

focused on the TiO bands and Na I lines in the optical–infrared (0.7–1.0 μm) (e.g., Friend et al. 1988). These searches proved insensitive to the secondary star in short-period CVs, although there were exceptions (e.g., Z Cha; Wade & Horne 1988). The relative insensitivity of optical searches to the secondary in short-period CVs is unsurprising, as short-period CVs are expected to possess late-type M-dwarf secondary stars.[1] These late-type M-dwarf stars have spectra which peak in the infrared (see Kleinmann & Hall 1986), and at optical wavelengths the light from the M dwarf is swamped by light from the accretion disc. Infrared searches for the secondary star in short-period CVs have largely focused on the *K* band (Dhillon 1997), with some success. Whilst the secondary star has proved relatively simple to find in dwarf novae above the period gap, where the contribution of the secondary in the *K* band is typically >75 per cent (Dhillon 1997), it has proved much more difficult to detect the secondary star in both nova-like variables and dwarf novae below the period gap. For these systems the contribution of the secondary to the infrared flux is usually much less (typically less than 25 per cent; Dhillon 1997). To find the secondary stars in these systems, a new strategy is required. In this paper we present the first results of a programme to detect secondary star features using the *J* band spectra of CVs.

Searching for secondary star features in the *J* band has certain

---

[1] The spectral type of the secondary star in a CV can be estimated from its orbital period, *P*, using the expressions $26.5 - 0.7P$ (for $P < 4\,\mathrm{hr}$) and $33.2 - 2.5P$ (for $P > 4\,\mathrm{hr}$), where G0 = 0, K0 = 10 and M0 = 20 (Smith & Dhillon 1998).

★ E-mail: php98spl@shef.ac.uk

© 2000 RAS

advantages over other wavelength ranges. First, observations in the near-infrared are plagued by a very high background. This is due to both thermal emission from the telescope, sky and instrument, and atmospheric emission from molecules (mostly OH^- and O_2) excited by daytime solar radiation, resulting in airglow which is both temporally and spatially variable (Ramsay, Mountain & Geballe 1992). This background is significantly lower in the J band than in K (16 mag arcsec^{-2} in J compared with 12 mag arcsec^{-2} in K; data for Mauna Kea, Hawaii). Second, in the late-type M dwarfs expected in post-period-gap CVs, there are more absorption features in the J band than in K, and these absorption features have larger equivalent widths than those in the K band (see, e.g., Jones et al. 1994). Third, the change in strength of absorption features with spectral type in late-type M dwarfs is more marked in the J band than in K (cf. table 2 in Dhillon & Marsh 1995 and Table 2 in this paper). This high sensitivity of absorption features to spectral type makes a secondary star detection in the J band a powerful constraint on models of the evolution of CVs below the period gap.

2   OBSERVATIONS

On the nights of 1998 August 8 and 9 we obtained spectra of the dwarf novae (DNe) WZ Sge, EF Peg and VY Aqr, the nova-like variable PX And, and the M dwarfs Gl644C and Gl866AB with the Cooled Grating Spectrometer (CGS4) on the 3.8-m United Kingdom Infrared Telescope (UKIRT) on Mauna Kea, Hawaii. CGS4 is a $1-5\,\mu m$ spectrometer containing an InSb array with 256×256 pixels. The 40 line mm^{-1} grating with the 300-mm camera gave a resolution of approximately 300 km s^{-1}. To cover the wavelength range $1.025-1.340\,\mu m$ required one grating setting, centred at $1.175\,\mu m$ (second order). Optimum spectral sampling and bad-pixel removal were obtained by mechanically shifting the array over two pixels in the dispersion direction in steps of 0.5 pixels. We employed the non-destructive readout mode of the detector to reduce the readout noise. In order to compensate for fluctuating atmospheric OH^- emission lines, we took relatively short exposures (typically 60 s) and nodded the telescope primary so that the object spectrum switched between two different spatial positions on the detector. The slit width was 0.6 arcsec (projecting to approximately 1 pixel on the detector) and was oriented at the parallactic angle throughout the second night. Observations of WZ Sge and Gl866AB were taken with a slit position angle of 0° to avoid light from a star close to WZ Sge falling on the slit. Using the UKIRT tip-tilt secondary, the seeing was around 0.5 arcsec on the first night, and dropped steadily from 0.8 to 0.4 arcsec on the second night. The humidity was low (10–20 per cent) throughout, and the sky was photometric for most of the run, although some high cirrus developed in the second half of the first night. A full journal of observations is presented in Table 1.

3   DATA REDUCTION

The initial steps in the reduction of the 2D frames were performed automatically by the CGS4 data reduction system (Daley & Beard 1994). These were the application of the bad-pixel mask, bias and dark-frame subtraction, flat-field division, interlacing integrations taken at different detector positions, and co-adding and subtracting nodded frames. Further details of the above procedures may be found in the review by Joyce (1992). In order to obtain 1D data, we removed the residual sky by subtracting a polynomial fit, and then extracted the spectra using an optimal extraction technique (Horne 1986). The next step was the removal of the ripple arising from variations in the star brightness between integrations (i.e., at different detector positions). These variations were due to changes in the seeing, sky transparency and the slight motion of the stellar image relative to the slit.

There were two stages to the calibration of the spectra. The first was the calibration of the wavelength scale using krypton arc lamp exposures. The second-order polynomial fits to the arc lines yielded an error of less than 0.0001 μm (rms). The final step in the spectral calibration was the removal of telluric features and flux calibration. This was performed by dividing the spectra to be calibrated by the spectrum of an F-type standard, with its prominent stellar features interpolated across. F-type stars were observed throughout the night, at different airmasses. In each case, the F star used was that which gave the best removal of telluric features, judged by the cancellation of the strong features around 1.14 μm. We then multiplied the result by the known flux of the standard at each wavelength, determined using a blackbody function set to the same effective temperature and flux as the standard. As well as providing flux-calibrated spectra, this procedure also removed telluric absorption features from the object spectra.

Table 1. Journal of observations. Each spectrum consists of 240 s total exposure time. Gaps between objects were used for arcs, flats and F-star spectra. An object is listed twice where such a gap broke continuous observation. The long gap between the observation of Gl866AB and WZ Sge is due to cloud. Observations of VY Aqr between 07:20 and 08:54 contained no useful information, due to very poor seeing. Spectral types are those given by Henry, Kirkpatrick & Simons (1994). Orbital phase is shown for WZ Sge using the ephemeris of Spruit & Rutten (1998), PX And using the ephemeris of Still, Dhillon & Jones (1995), and VY Aqr using the ephemeris of Thorstensen & Taylor (1997). The orbital period for EF Peg is estimated from the superhump period (Howell et al. 1993).

| Object	$\lambda_{central}$ (μm)	Date	UT start	UT end	No. of Spectra	Period (days)	Phase start	Phase end	Spectral Type	J band mag.
WZ Sge	1.175	08/08/98	06:40	08:33	24	0.0567	0.24	1.43		15.3
WZ Sge	1.175	08/08/98	08:47	10:36	24	0.0567	1.80	2.97		15.3
Gl866AB	1.175	08/08/98	10:56	11:27	4				M5V	
WZ Sge	1.175	08/08/98	12:40	13:50	14	0.0567	4.66	5.19		15.3
PX And	1.175	08/08/98	14:09	15:04	12	0.1464	0.61	0.82		14.2
Gl644C	1.175	09/08/98	06:20	06:45	4				M7V	
VY Aqr	1.175	09/08/98	07:20	08:54	20	0.0635	0.81	1.19		14.2
VY Aqr	1.175	09/08/98	09:22	10:53	20	0.0635	1.50	2.36		14.2
EF Peg	1.175	09/08/98	11:36	13:09	20	0.0837				
EF Peg	1.175	09/08/98	13:33	14:46	16	0.0837				
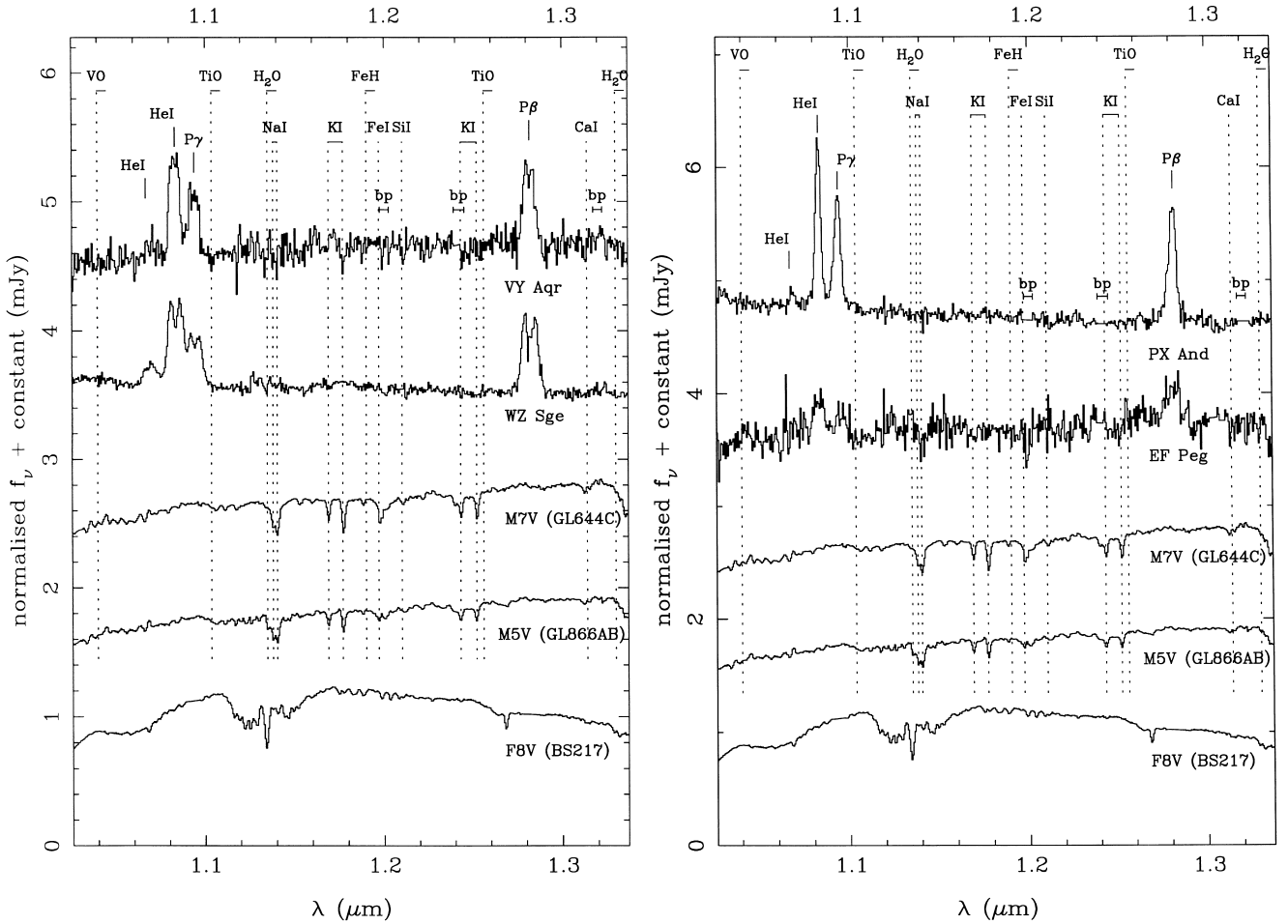
Figure 1. Left-hand side: Average J band spectra of the short-period DNe WZ Sge and VY Aqr, and the M dwarfs Gl644C and Gl866AB. Right-hand side: Average J band spectra of the short-period DN EF Peg, the nova-like variable PX And, and the M dwarfs Gl644C and Gl866AB. For both plots, the spectra have been normalized by dividing by the flux at 1.3 μm and then offset by adding a multiple of 0.9 to each spectrum. Also shown is the spectrum of an F8V star, normalized by dividing by the flux at 1.3 μm, which indicates the location of telluric features.

Table 2. Wavelengths, equivalent widths and velocity widths of the most prominent lines in the J band spectra of the nova-like variable PX And, the DNe WZ Sge, EF Peg and VY Aqr, and the M dwarfs Gl644C and Gl866AB. The line identifications were made using the lists and spectra of Kirkpatrick et al. 1993 (marked [a]), Joyce et al. 1998 (marked [b]), Jones et al.1994 (marked [c]), Jones et al. 1996 (marked [d]), Tinney, Mould & Reid 1993 (marked [e]), Lang 1986 (marked [f]) and the UKIRT online documentation (marked [g]). Equivalent widths for the water band around 1.34 μm were measured in the range 1.32–1.34 μm. The vertical bars following lines of similar wavelength indicate that the measurements apply to the entire blend. Wavelengths for VO, TiO, H_2O and FeH refer to the band heads, or the edge of the band, if headless. The two-letter codes indicate either that the line is not present (np), or that the line is present but is not measurable (nm).

Line	λ (μm)	WZ Sge EW Å	WZ Sge FWHM km s^{-1}	EF Peg EW Å	EF Peg FWHM km s^{-1}	VY Aqr EW Å	VY Aqr FWHM km s^{-1}	PX And EW Å	PX And FWHM km s^{-1}	Gl866AB EW Å	Gl866AB FWHM km s^{-1}	Gl644C EW Å	Gl644C FWHM km s^{-1}
He I	1.0830[f]	67 ± 1	2300 ± 100	28 ± 3	1500 ± 300	53 ± 2	1500 ± 100	46 ± 1	890 ± 30	np	np	np	np
Pa-γ	1.0938[f]	34 ± 1	2100 ± 100	15 ± 3	1700 ± 300	30 ± 2	1500 ± 100	51 ± 1	1200 ± 30	np	np	np	np
Pa-β	1.2818[g]	69 ± 1	2400 ± 100	30 ± 3	2100 ± 300	40 ± 3	1600 ± 100	58 ± 2	1200 ± 30	np	np	np	np
He I	1.0668[g]	11 ± 1	nm	nm	nm	np	np	np	np	np	np	np	np
VO	1.0400[b]	np	np	np	np	np	np	np	np	nm	nm	nm	nm
TiO	1.1035[b]	np	np	np	np	np	np	np	np	nm	nm	nm	nm
H₂0	1.1350[b]												
NaI	1.1381[c]												
NaI	1.1404[c]	np	np	np	np	np	np	np	np	−14 ± 1	nm	−10 ± 1	nm
KI	1.1690[c]												
KI	1.1773[c]	np	np	np	np	np	np	np	np	−6 ± 1	nm	−12 ± 1	nm
FeH	1.1900[a]												
FeI	1.1970[d]	np	np	np	np	np	np	np	np	−7 ± 1	nm	−15 ± 1	nm
SiI	1.2100[e]	np	np	np	np	np	np	np	np	−2 ± 1	nm	nm	nm
KI	1.2432[c]												
KI	1.2522[c]	np	np	np	np	np	np	np	np	−10 ± 1	nm	−21 ± 1	nm
TiO	1.2560[b]	np	np	np	np	np	np	np	np	−1 ± 1	nm	nm	nm
CaI	1.3140[c]	np	np	np	np	np	np	np	np	−1 ± 1	nm	−1 ± 1	nm
H₂O	1.3400[c]	np	np	−14 ± 4	nm	−17 ± 4	nm	np	np	−10 ± 1	nm	−14 ± 1	nm

4   RESULTS

Fig. 1 shows the 1.025–1.340 μm averaged spectra of the short-period DNe WZ Sge and VY Aqr (left-hand side) and the 1.025–1.340 μm averaged spectra of the short-period DN EF Peg and the nova-like variable PX And (right-hand side), together with the spectra of M7 and M5 field dwarfs. We also show the spectrum of an F8V star, which indicates the location of telluric absorption features; spectral features within the strongest absorption bands are highly uncertain. The location of bad pixels are labelled by a bar showing the extent of the anomaly and the label 'bp'. In Table 2 we list the wavelengths, equivalent widths and velocity widths of the most prominent spectral lines identified in Fig. 1.

4.1   Accretion disc features

The spectra of WZ Sge and VY Aqr (Fig. 1) are dominated by the strong, double-peaked emission lines of He I, Paschen-γ and Paschen-β. Also seen is a small broad peak around 1.07 μm. This is identified as the He I line at 1.0668 μm. The broad, double-peaked nature of these lines indicates an origin in the accretion disc. The full-width at half-maxima (FWHM) for WZ Sge are in agreement with those presented by Dhillon et al. (in preparation), who find a FWHM for the Brackett-γ line of 2200 km s^{-1}. The FWHM for VY Aqr are in good agreement with Thorstensen & Taylor (1997), who find a FWHM of 1550 km s^{-1} for Hα. We measured the separation of the double-peaked emission lines for VY Aqr and WZ Sge. For WZ Sge the peak separations were 1400 ± 100, 1300 ± 100 and 1400 ± 100 km s^{-1} for He I, Pγ and Pβ respectively. These values are in good agreement with values for the peak separation derived from optical data, e.g., 1380 km s^{-1} for Hα (Gilliland, Kemper & Suntzeff 1986). For VY Aqr the peak separations were 700 ± 100, 800 ± 150 and 900 ± 100 km s^{-1} for He I, Pγ and Pβ respectively. These peak separations for VY Aqr are in good agreement with Thorstensen & Taylor, who find a peak separation of 930 km s^{-1} for Hα.

The spectrum of PX And (Fig. 1) is dominated by the strong, single-peaked emission lines of He I, Paschen-γ and Paschen-β, typical of the SW Sex stars of which PX And is a member (Still, Dhillon & Jones 1995). The FWHM for PX And are consistent with the values given by Still et al., who find FWHM of 930–1030 km s^{-1} for He I emission and 1080–1600 km s^{-1} for the Balmer lines.

The spectrum of EF Peg (Fig. 1) also shows strong emission lines, although the signal-to-noise ratio is too low to say if these are single- or double-peaked. The large velocity widths of the emission lines in EF Peg suggest an accretion disc origin.

4.2   Secondary star features

The spectrum of VY Aqr shows increasing flux towards the red end of the spectrum, with a continuum slope of $(7.4 \pm 0.4) \times 10^{-1}$ mJy μm^{-1}, suggesting that the secondary star makes a significant contribution to the continuum light in VY Aqr (cf. the slope of the M dwarfs in Fig. 1). The continuum in VY Aqr also exhibits a change in slope at ~1.1 μm. This feature is also present in the spectra of the M dwarfs. The spectrum of VY Aqr also shows a tentative detection of secondary star absorption features, particularly the headless water band seen at 1.33 μm. Likewise, the EF Peg continuum shows increased flux at the red end of the spectrum, with a continuum slope of $(5.7 \pm 0.8) \times$
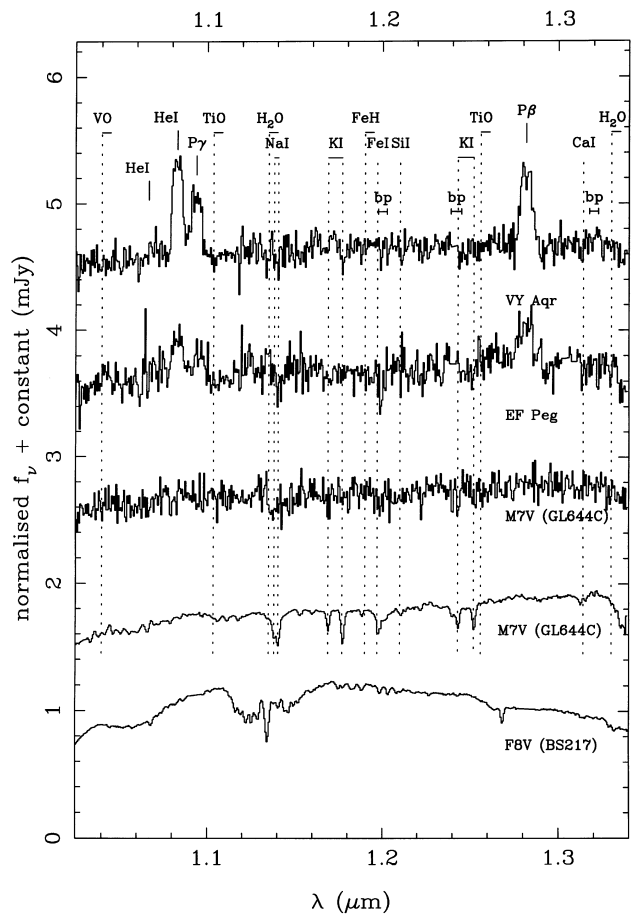

Figure 2. Average *J*-band spectra of the short-period DNe VY Aqr and EF Peg, and the M dwarf Gl644C. The spectra have been normalized by dividing by the flux at 1.3 μm and then offset by adding a multiple of 0.9 to each spectrum. One spectrum of Gl644C has been divided by 1.7, in an attempt to match the appearance of the absorption feature at 1.33 μm to that seen in VY Aqr, and noise has then been added to the spectrum in order to match the signal-to-noise ratio to that of the DNe spectrum. Also shown is the spectrum of an F8V star, normalized by dividing by the flux at 1.3 μm, which indicates the location of telluric features.

10^{-1} mJy μm^{-1} and, like the spectrum of VY Aqr, EF Peg also shows a tentative secondary star detection through the water band at 1.33 μm. The EF Peg continuum also shows a change in slope at ~1.1 μm, in common with VY Aqr and the M dwarfs. The detection of the water band in EF Peg and VY Aqr should be considered carefully: the spectra do not show any of the other absorption features visible in the spectra of the M dwarfs – although it is possible they are lost in the noise. Fig. 2 shows the spectra of the DNe EF Peg and VY Aqr, together with two spectra of the M dwarf Gl 644c. One spectrum of Gl 644c has been divided by 1.7 in order to weaken the appearance of the spectral lines (the correct amount was judged by attempting to match the appearance of the 1.33-μm water feature to that seen in VY Aqr). This spectrum has then had noise added in order to match the signal-to-noise ratio to that of the DNe spectra. Absorption features are barely discernible in this spectrum. This shows that absorption features from the secondary star are probably hidden by noise in the CV spectra. Furthermore, the most prominent absorption features fall at the same wavelengths as the strongest telluric features and bad pixels, and any features in these regions are inevitably more uncertain. In addition, the water feature at

1.33 µm occurs only in concurrence with the red continuum seen in VY Aqr and EF Peg, and does not appear in the spectrum of WZ Sge, for example. We believe that this constitutes a body of evidence for the detection of the secondary star in VY Aqr and EF Peg. This is discussed further in Section 5. Unfortunately, without detection of more absorption features and the observation of more field-dwarf templates we are unable to determine the spectral types of the secondary stars in EF Peg and VY Aqr.

There is no evidence for the secondary stars in the spectra of WZ Sge and PX And, which show a blue continuum without any changes in slope or absorption features.

Table 3. The contributions of the secondary stars to the total *J*-band flux.

Object	Secondary Contribution	Error	M dwarf used	Mag. of Secondary
WZ Sge	≤10%	5%	M7	≥16.2
PX And	≤20%	5%	M5	≥15.4
EF Peg	65%	15%	M7	16.7 ± 0.5
VY Aqr	70%	15%	M5	15.7 ± 0.5

4.3 Secondary star contributions and distances

Table 3 shows the contribution of the secondary star to the total flux of each CV. Percentages were calculated by normalizing the average spectra of both the CV and M-dwarf template. An increasing fraction of the M-dwarf spectrum was then subtracted from the CV spectrum until spectral features in the CV spectrum were removed or absorption features from the M dwarf appeared in emission. The fraction at which this occurs gives the contribution of the secondary star to the total flux. Where no secondary star features are present, this represents an upper limit to the contribution of the secondary star.

The contributions were found to vary, depending upon which M-dwarf template was used. It follows that systematic error could be introduced through using a template whose spectral type differs greatly from the actual spectral type of the secondary star.

The strongest features in the template spectra increase in strength with spectral type. Hence templates of earlier spectral type give a higher contribution than those later in the spectral sequence. Hence, for WZ Sge and PX And, where the earliest spectral type consistent with the spectral type–orbital period relation in Smith & Dhillon
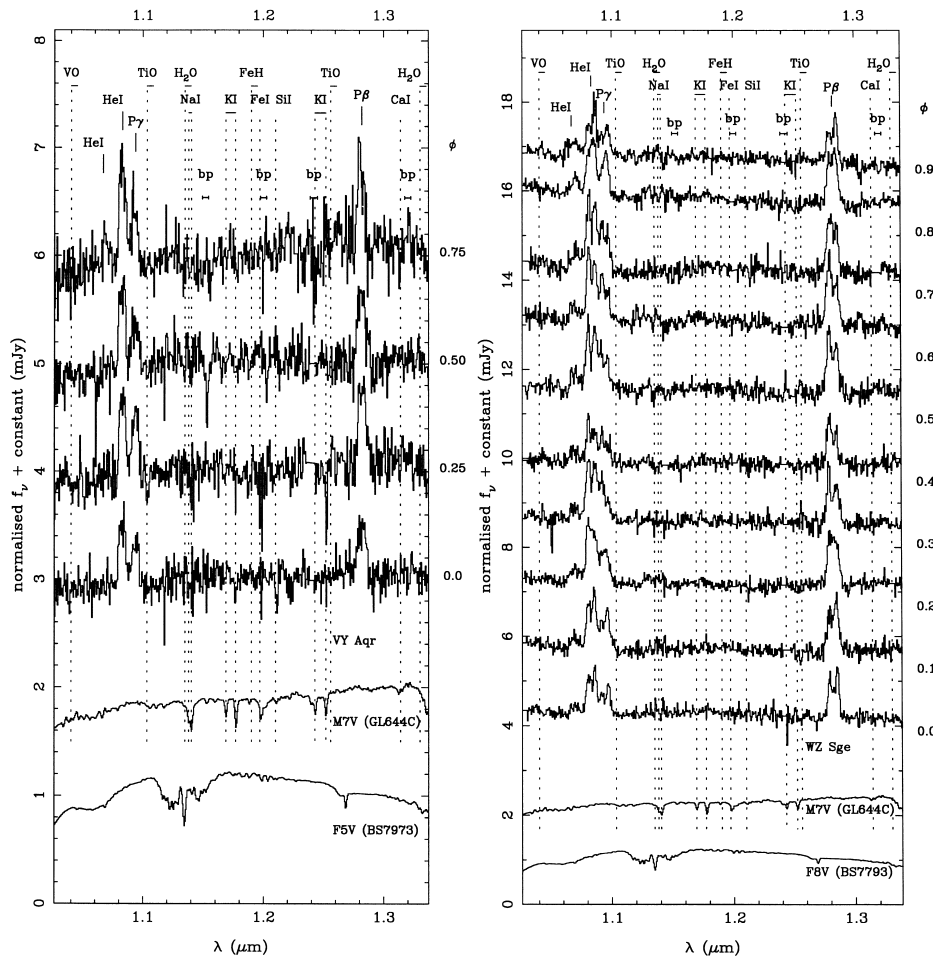

Figure 3. Left-hand side: Time-resolved *J*-band spectra of the short-period DN VY Aqr, and spectra of the M dwarf Gl644C. Orbital phase is shown on the right-hand side of the plot, using the ephemeris of Thorstensen & Taylor (1997) – i.e without applying the phase offset described in Section 4.5. Right-hand side: Time-resolved *J*-band spectra of the short-period DN WZ Sge, and spectra of the M dwarf. Orbital phase is shown on the right-hand side of the plot, using the ephemeris of Spruit & Rutten (1998). In both plots the spectra have been normalized by dividing by the flux at 1.3 µm. The spectra were then offset by a multiple of 1.0 for VY Aqr and 1.4 for WZ Sge. Also shown is the spectrum of an F8V star, normalized by dividing by the flux at 1.3 µm, which indicates the location of telluric features. The location of bad pixels is labelled by a bar showing the extent of the anomaly and the label 'bp'.

(1998) was used, we have derived strict upper limits to the contribution of the secondary star to the J band light.

In VY Aqr and EF Peg, we used the M dwarf which was able to correct the H_2O band at $1.33\,\mu m$ and flatten the continuum without introducing spectral features in emission. It would have been apparent if the spectral type of the template used was too late, as the K I feature at $\sim 1.17\,\mu m$ increases in strength more rapidly with spectral type than the H_2O feature at $1.33\,\mu m$. Hence a template with too late a spectral type would not be able to correct the water feature without introducing the K I feature in emission. Templates whose spectral types are too early would give a larger value for the secondaries star contribution. However, the spectral type of the secondaries in EF Peg and VY Aqr should be later than M5V. Hence we believe that the contributions derived for these stars are reliable. The errors shown in Table 3 are the discrepancies between the values obtained with the two M-dwarf templates, and hence reflect the uncertainty resulting from the unknown spectral type.

The contributions of the secondary star will also be affected by systematic error due to flux from the disc if an emission feature corrupts the water band at $1.33\,\mu m$. This is not thought to be the case.

We find an upper limit to the secondary star contribution to the J band light in WZ Sge of 10 per cent, consistent with Ciardi et al.
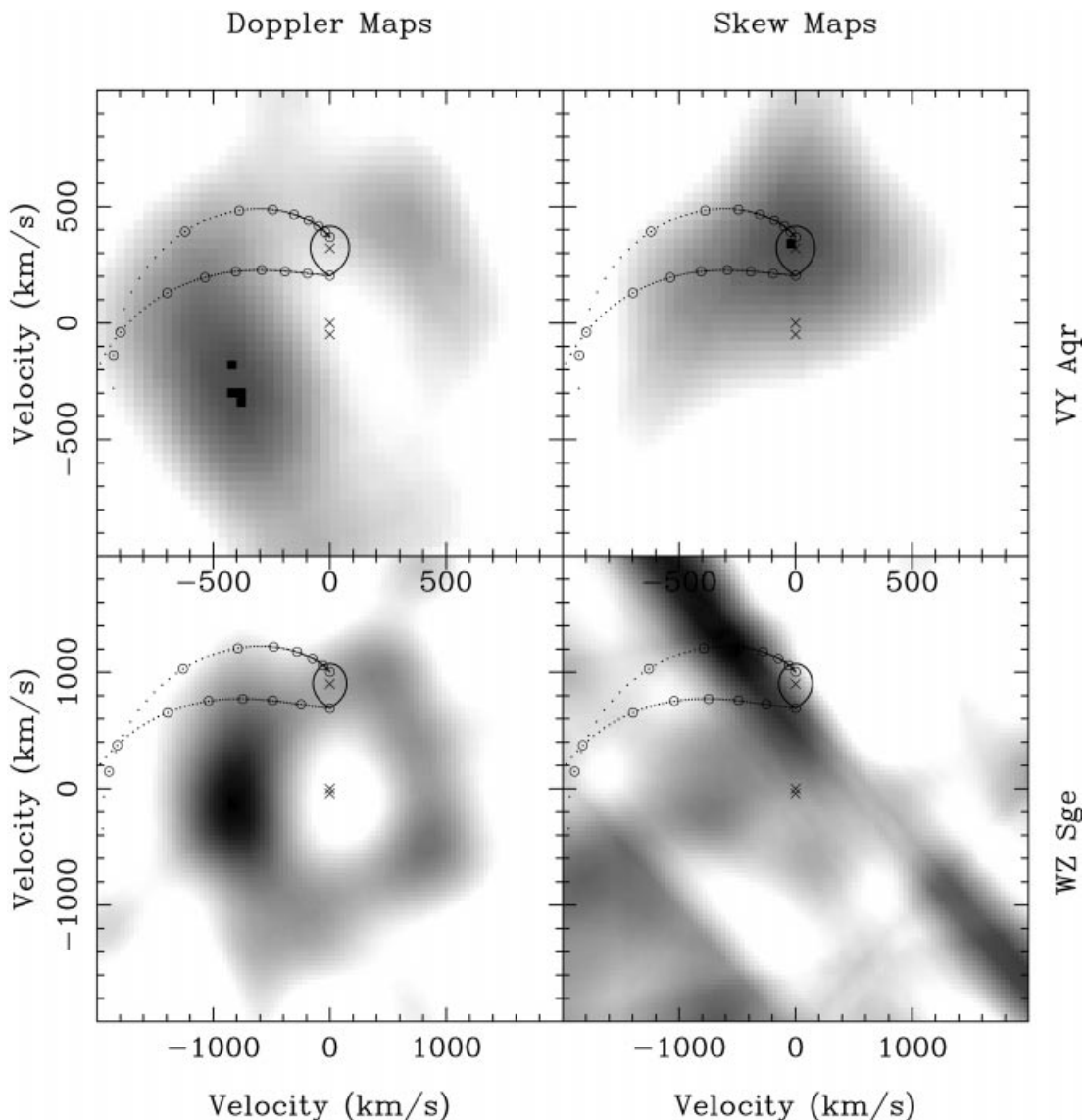

Figure 4. (Top) Left-hand panel: The Doppler map of the Paschen-β line in VY Aqr. Right-hand panel: The skew map of VY Aqr, made with the M dwarf Gl866AB (M5V). The value of K_R is given by $K_R^2 = K_X^2 + K_Y^2$ where K_X and K_Y are found from the skew map by the position of the peak. Both maps have had a phase correction of -0.28 made to the ephemeris of Thorstensen & Taylor (1997). The predicted position of the secondary star, the path of the gas stream (lower curve) and the Keplerian velocity at the gas stream (upper curve) are marked on both maps, using the value of q derived in the text. The three crosses on the maps are, from top to bottom, the centre of mass of the secondary star, the system (at zero velocity) and the white dwarf. The circles plotted on the gas stream represent (from left to right) increasing distance from the white dwarf (in steps of one-tenth of the distance to the inner Lagrangian point, L_1). (Bottom) Left-hand panel: The Doppler map of the Paschen-β line in WZ Sge. Right-hand panel: The skew map of WZ Sge, made with the M dwarf Gl866AB (M5V). The predicted position of the secondary star, the path of the gas stream, and the Keplerian velocity at the gas stream are marked on both maps, along with the centre of mass of the system components, in an identical fashion to that above, using the system parameters of Spruit & Rutten (1998).

(1998), who model the relative contributions to the near-infrared emission in WZ Sge and find that the secondary star should contribute ≈ 20 per cent of the near-infrared flux, although their models suggest that this figure is lower (perhaps ≈ 10 per cent) in the *J* band.

If the *J* band magnitude for the CV is known, it is possible to derive the apparent *J* band magnitude of the secondary. In principle, this apparent magnitude can then be used to estimate the distance to the CV, by comparison with the absolute magnitude of a field-dwarf of appropriate spectral type. In the cases where the secondary has not been detected, this value represents a lower limit to the distance involved. *J* band magnitudes for WZ Sge, VY Aqr and PX And are 14.2, 15.3 and 14.2 respectively (Mark Huber, private correspondence). The *J* band magnitude of EF Peg is 16.1 (Mark Huber, private correspondence). This gives a *J* band magnitude of 15.7 ± 0.5 for the secondary in VY Aqr, 16.7 ± 0.5 for the secondary in EF Peg, and upper limits of 16.2 and 15.4 for the *J* band magnitudes of the secondaries in WZ Sge and PX And respectively. Unfortunately, we are unable to give distances to these CVs, as the absolute *J* band magnitude of M dwarfs varies rapidly with spectral type – cf. $M_J = 6.56$ for M5V with $M_J = 8.75$ for M7V (Bessell 1991) – a reliable spectral type determination is necessary before distances can be estimated. As an aside, it is worth noting that both Smak (1993) and Spruit & Rutten (1998) find a distance to WZ Sge of 48 pc, which, through the analysis above and the data in Bessell (1991), would constrain the spectral type of the secondary to be later than M7.5V, consistent with Ciardi et al. (1998), who find that the secondary star in WZ Sge is cooler than 1700 K.

4.4 Time-resolved spectra

Fig. 3 shows the *J* band time-resolved spectra of VY Aqr (left-hand side) and the *J* band time-resolved spectra of WZ Sge (right-hand side) together with the spectra of M7 and M5 field dwarfs. The majority of ephemerides for WZ Sge are for mid-eclipse of what is believed to be the bright spot. In this paper, WZ Sge is phased according to the ephemeris of Spruit & Rutten (1998), whose binary phase zero is corrected to represent mid-eclipse of the white dwarf.

The emission lines in VY Aqr vary considerably over the orbit. The H_2O feature at $1.33\,\mu m$ also shows variation with phase. It does not appear to be present at phase $\phi = 0.0$. We have been unable to account for this variation; possible causes are discussed in Section 5. There is no evidence for a change in the continuum slope in VY Aqr with orbital phase, with the slope always remaining within one standard error of the mean, given in Section 4.2.

The emission lines in WZ Sge show a strong variation with orbital phase. There is a reduction in line strength at $\phi \approx 0.9$ and $\phi \approx 0.0$, the latter corresponding to primary eclipse. The lines appear single-peaked at $\phi \approx 0.3$ and $\phi \approx 0.8$.

Time-resolved spectra were not obtained for EF Peg and PX And.

4.5 Skew mapping and Doppler tomography

Skew maps were produced of both WZ Sge and VY Aqr. Skew mapping is a tomographic technique used to extract a value for the radial velocity of the secondary star, K_R. It is particularly useful when the spectral features are too weak for conventional cross-correlation techniques to work. It is described in detail in Smith, Cameron & Tucknott (1993), and has been successfully employed

by Smith, Dhillon & Marsh (1998). We compared regions of the spectra unaffected by emission lines with the spectra of our M5 and M7 dwarf stars. The first step was to remove the continuum from the spectrum of both the CV and the template stars. This is done by dividing by a first-order polynomial fit, and then subtracting a higher order fit to the continuum. This ensures that line strength is preserved along the spectrum. Each of the time-resolved CV spectra were then cross-correlated with the template star spectra, giving a time-series of cross-correlation functions (CCFs) for each template. The skew maps were then generated by back-projecting the CCFs, in an identical fashion to time-resolved spectra in standard Doppler tomography (Marsh & Horne 1988). If there is a detectable secondary star, we would expect a peak at $(0, K_R)$ in the skew map.

Fig. 4 shows the skew map of VY Aqr, made with Gl866AB and a standard Doppler map of the Paschen-β line in VY Aqr. When we first performed the skew mapping of VY Aqr, a strong peak appeared in the lower right-hand quadrant. Because we cross-correlate only with absorption features in the M-dwarf template, it is unlikely that the peak could be from anything but the secondary star, and so we believe that the unusual position of the peak is due
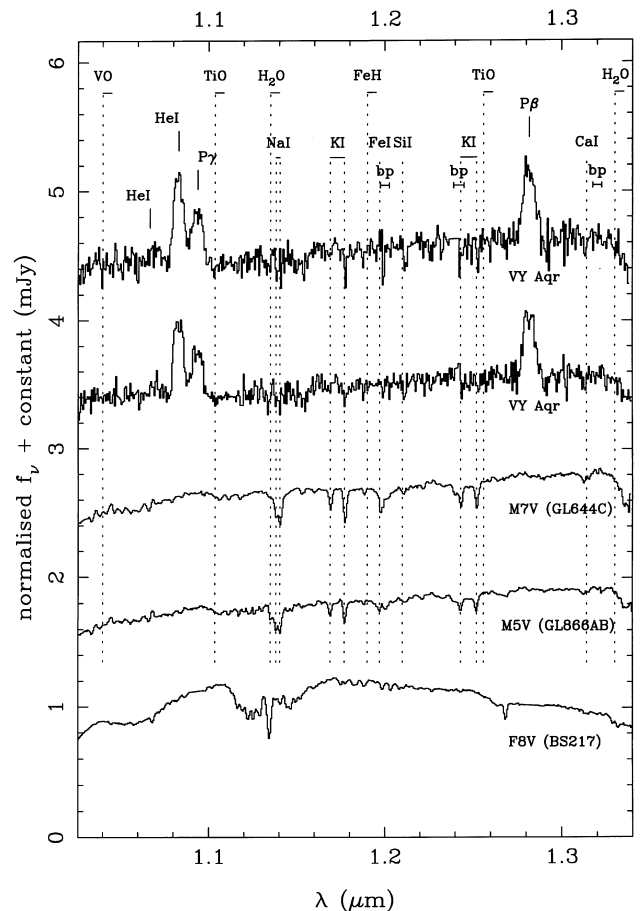

Figure 5. Average *J*-band spectra of the short-period DNe VY Aqr and the M dwarfs Gl644C and Gl866AB. The upper spectrum of VY Aqr has been corrected for the radial velocity of the secondary star, and represents an average spectrum in the rest frame of the secondary star. The spectra have been normalized by dividing by the flux at $1.3\,\mu m$ and then offset by adding a multiple of 0.9 to each spectrum. Also shown is the spectrum of an F8V star, normalized by dividing by the flux at $1.3\,\mu m$, which indicates the location of telluric features.

to a discrepancy between the ephemeris of Thorstensen & Taylor (1997) and the actual ephemeris at the time of our observations. Thorstensen & Taylor give their error in the period as ± 0.00004 d, allowing for a discrepancy of up to seven orbits between the calculated and actual phases at the time of observation. Hence both maps of VY Aqr have had a phase correction of -0.28 applied to the ephemeris of Thorstensen & Taylor, in order to move the peak in the skew map to the expected position on the $K_X = 0$ axis.

The skew map of VY Aqr shows a significant peak, yielding a value of $K_R = 320 \pm 70$ km s^{-1}. As a check, the time-resolved spectra of VY Aqr were shifted to correct for the radial velocity of the secondary star, and then averaged. The results are shown in Fig. 5. Secondary star absorption features are clearly visible in the corrected spectrum, which also shows a much stronger and sharper water band. We conclude that our value of K_R is appropriate, and not an artefact of the skew-mapping process. Thorstensen & Taylor (1997) find $K_W = 49 \pm 4$ km s^{-1} from Hα, giving a value for the mass ratio of the system of $q = 0.15 \pm 0.04$. This value of q is consistent with the precessing-disc model for SU UMa stars (Whitehurst 1988), to which VY Aqr belongs. We are unable to derive component masses, as the inclination of the system is uncertain (Augusteijn 1994). Furthermore, it should be noted that K_W, when derived from emission lines, does not always reflect the true motion of the white dwarf.

The Doppler map of VY Aqr shows a faint ring corresponding to disc emission, and a peak we associate with the bright spot at $(-500, -300)$ km s^{-1}. Assuming that our phase offset is correct, we find that the bright spot in VY Aqr is located downstream from the stream impact region. This is consistent with the optical and infrared Doppler maps of WZ Sge (see below), and with infrared

eclipse maps of IP Peg, which show that the infrared continuum bright spot can also appear downstream of its optical counterpart (Froning et al. 1999). Work is in progress to determine if this is a common feature in infrared accretion disc maps (Littlefair & Dhillon, in preparation). This consistency with other infrared maps, as well as consistency with the radial velocity curves and light curves presented later in this paper, gives us confidence that our phase correction is appropriate.

Fig. 4 shows a standard Doppler map of the Paschen-β line in WZ Sge, along with a skew map of WZ Sge, made with Gl866AB. The Doppler map shows faint accretion disc structure, and is dominated by emission from the bright spot at $(-800, -200)$ km s^{-1}. Spruit & Rutten (1998) found that the optical bright spot was located downstream from the stream impact region. Using their ephemeris, we find that the infrared bright spot is not aligned with its optical counterpart, but is located further downstream from the stream impact region, consistent with our results for VY Aqr. The skew map of WZ Sge shows no peak from the secondary star, but a bright streak corresponding to a large value of the cross-correlation function at $\phi \approx 0.9$. It is possible that this is due to correlation with secondary star features, especially as it occurs near eclipse, although the absence of a strong correlation at other phases, and the fact that it is not exactly at $\phi = 0$ makes this unlikely.

4.6 Light curves

Fig. 6 shows equivalent width (EW) light curves for WZ Sge and VY Aqr. The light curves have been folded over two complete orbits for clarity. They show a large amount of scatter, due to noise in the spectra, and hence should be interpreted with caution. Both
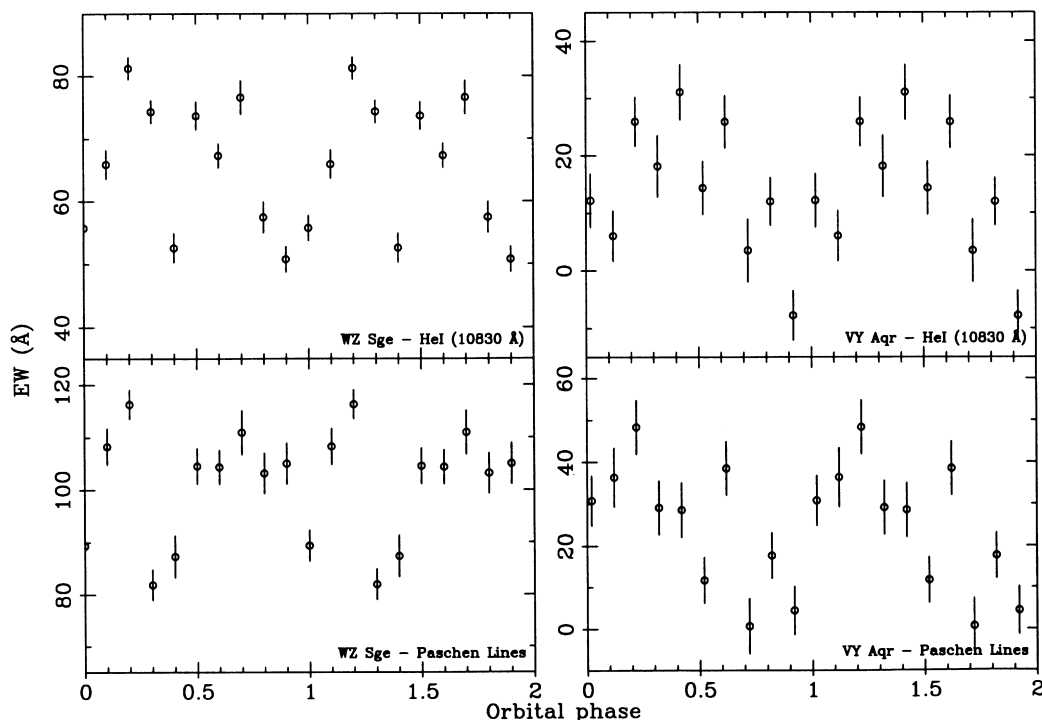

Figure 6. Emission-line equivalent width (EW) light curves of WZ Sge and VY Aqr. EWs were calculated from the He I (10830 Å) line and from the sum of the Paschen lines (Pγ + Pβ). The He I line was separated from the Paschen-γ line by measuring the EW up to a point at the middle of the blend. Hence the He I light curve is contaminated with a small amount of light from Paschen-γ and vice versa. The light curves have been folded over two complete orbits for clarity. Phases for WZ Sge are from the ephemeris of Spruit & Rutten (1998); phases for VY Aqr are shown using the ephemeris of Thorstensen & Taylor (1997), with a correction of -0.28 applied.
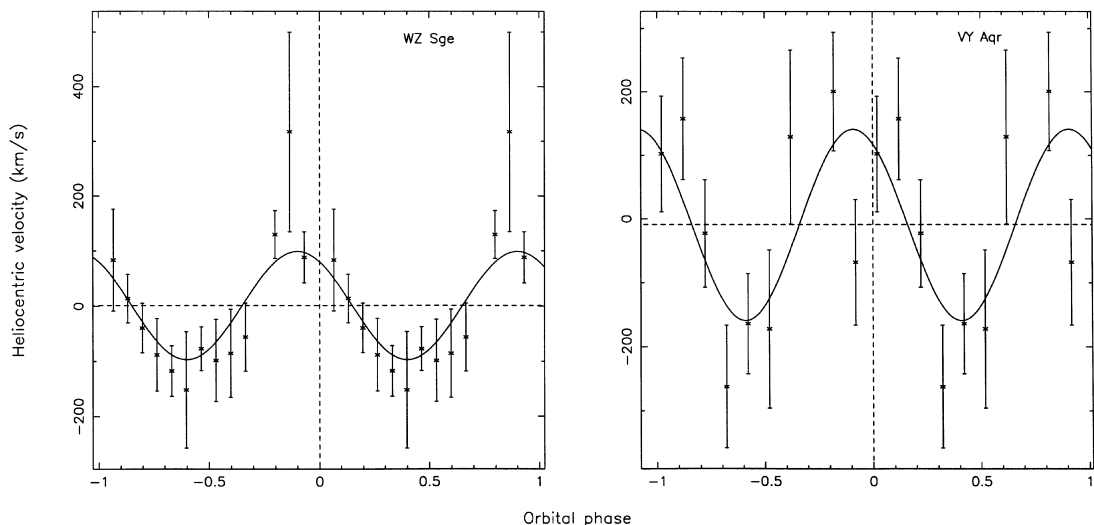
Figure 7. Radial velocity curves of Paschen-β for WZ Sge and VY Aqr, measured using a double-Gaussian fit with Gaussian separations of $1600\,\mathrm{km\,s^{-1}}$ (VY Aqr) and $2000\,\mathrm{km\,s^{-1}}$ (WZ Sge). Points at primary eclipse are omitted from the plot. The curves are folded over two complete orbits for clarity. Also shown are the fits to the curves (solid line) and the systemic velocities (horizontal dashed line). Phases for WZ Sge are from the ephemeris of Spruit & Rutten (1998); phases for VY Aqr are shown using the ephemeris of Thorstensen & Taylor (1997), with a correction of -0.28 applied.

the He I ($10830\,\text{Å}$) and the Paschen-line light curves in WZ Sge show an eclipse at $\phi \approx 0$.

The VY Aqr light curves show a systematic variation in brightness, with a minimum brightness occurring at $\phi \approx 0.9$ in the He I lines and at $\phi \approx 0.75$ in the Paschen lines, where we have applied the correction of -0.28 to the ephemeris of Thorstensen & Taylor (1997). Such a variation could be produced either by obscuration of the bright spot by an optically thick disc, or by self-obscuration of an optically thick bright spot whose outer edge is brighter than the inner. Doppler maps of the He I emission in VY Aqr show emission from a bright spot which is not aligned with the Paβ emission. This explains the lag between the He I light curve and the Paschen-line light curve. The presence of any variation at the orbital period in the light curves is surprising, as Patterson et al. (1993) found no variations on the orbital period in the optical continuum light curve of VY Aqr. Further infrared photometry seems desirable.

4.7 Radial velocity curves

The time-resolved spectra were continuum-subtracted and binned on to a constant velocity interval scale. In order to measure the radial velocities, we applied the double-Gaussian method of Schneider & Young (1980) to the Paschen-β line. This technique is sensitive mainly to the motion of the line wings and should therefore reflect the motion of the white dwarf with the highest reliability. The Gaussians were of width $500\,\mathrm{km\,s^{-1}}$ (FWHM), and we varied their separation from 600 to $2400\,\mathrm{km\,s^{-1}}$. We then fitted

$$V = \gamma - K \sin(\phi - \phi_0) \qquad (1)$$

to each set of measurements, omitting the points at primary eclipse. Examples of the radial velocity curves obtained for WZ Sge and VY Aqr are shown in Fig. 7.

The results of the radial velocity analysis are displayed in the form of a diagnostic diagram in Fig. 8. By plotting K, its fractional error σ_K/K, γ and ϕ_0 as functions of the Gaussian separation it is possible to select the value of K which most closely matches K_W
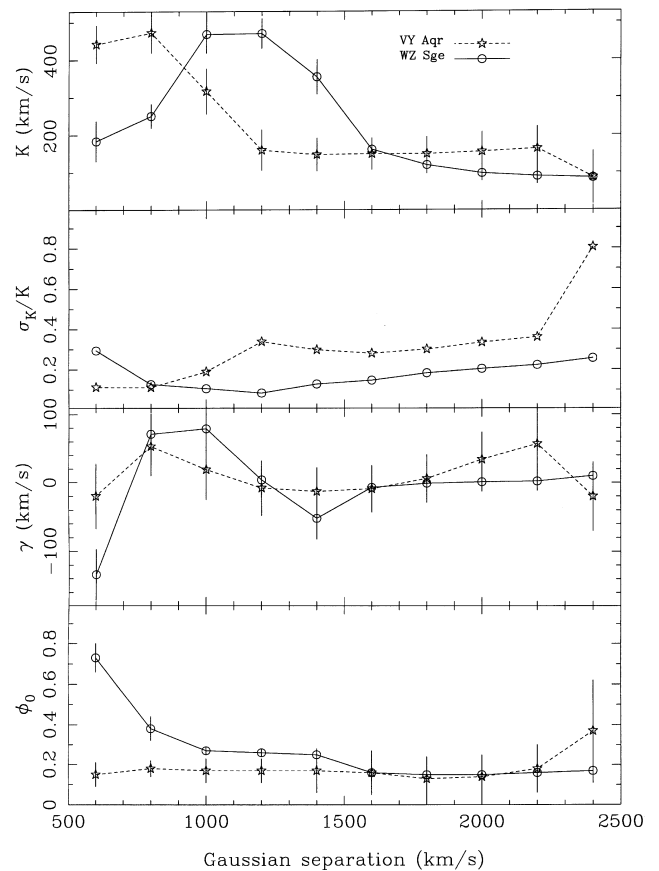

Figure 8. Diagnostic diagrams for WZ Sge and VY Aqr based on the double-Gaussian fits to Paschen-β. Phases for WZ Sge are from the ephemeris of Spruit & Rutten (1998); phases for VY Aqr are shown using the ephemeris of Thorstensen & Taylor (1997), with a correction of -0.28 applied.

(Shafter, Szkody & Thorstensen 1986). If emission is disc-dominated, one would expect K to asymptotically approach K_W when the Gaussian separation becomes sufficiently large. Furthermore, one would expect ϕ_0 to approach 0.

© 2000 RAS, MNRAS **313**, 117–128

For WZ Sge it can be seen that the phase shift ϕ_0 does indeed fall towards 0 with increasing Gaussian separation. The value of K steadily drops, reaching its lowest value at around $K = 85 \pm 20\,\mathrm{km\,s}^{-1}$. At this point the phase shift is 0.17 ± 0.06 and not zero, as is typical for this sort of measurement in CVs (see, e.g., section 2.7.6 in Warner 1995 for a discussion). This phase shift introduces doubt about the validity of adopting this figure for K_W. Several authors have attempted to measure K_W in WZ Sge with optical values ranging from 40 to $70\,\mathrm{km\,s}^{-1}$ for Hα and from 60 to $80\,\mathrm{km\,s}^{-1}$ for Hβ – see Skidmore (in preparation). Spruit & Rutten (1998), using a light centres method which attempts to correct for contamination by light from the hotspot, find a value for Hα of $40 \pm 10\,\mathrm{km\,s}^{-1}$. K band infrared studies of WZ Sge yield a value for K, from the Brγ line, of $108 \pm 15\,\mathrm{km\,s}^{-1}$ (Skidmore, in preparation). Our value is compatible with the higher optical values.

For VY Aqr the phase shift does not fall to zero, instead remaining roughly constant at $\phi_0 \approx 0.16$, again typical for this type of measurement. The value of K remains fairly constant at $150 \pm 50\,\mathrm{km\,s}^{-1}$. This value is inconsistent with the value obtained by Thorstensen & Taylor (1997) of $K_W = 49 \pm 4\,\mathrm{km\,s}^{-1}$ for Hα.

It is not easy to read reliable values of K_W from our diagnostic diagram. Thus, in an attempt to obtain reliable values for K_W for both VY Aqr and WZ Sge, we employed a modified version of the light centres method, described by Marsh (1988). In the co-rotating coordinate frame, the white dwarf has velocity $(0, -K_W)$, and any symmetric emission (e.g., from the disc) would be centred at that point. By plotting $K_X = -K \sin \phi_0$ against $K_Y = -K \cos \phi_0$ for the different radial velocity fits, we find that the points move closer to the K_Y axis with increasing Gaussian separation. This is because at large separations the fits are dominated by the line wings, which should be formed in the symmetric, inner disc. An extrapolation of the points to the K_Y axis should give a measurement of K_W. Such a light centres diagram is presented in Fig. 9.

The light centres in both plots seem to cluster at the edges of the bright spots as the Gaussian separation increases. Hence we are unable to extrapolate to $K_X = 0$, and therefore unable to estimate K_W for WZ Sge and VY Aqr.

5   DISCUSSION

We consider here the reality of the secondary star detection in VY Aqr and EF Peg. The secondary star detection is based on three points of evidence: the continuum slope, the presence of the water band at $1.33\,\mu\mathrm{m}$, and the success of the skew mapping technique. We consider these points in turn.

(i) VY Aqr has a red continuum. The continuum shows a change in slope around $1.1\,\mu\mathrm{m}$, a feature shared by the M-dwarf spectra. In fact, the continuum shape in VY Aqr strongly resembles that of the M dwarfs. As the accretion disc and white dwarf are expected to have a blue continuum, it is reasonable to ascribe the red continuum seen in VY Aqr to light from the secondary star. This does not necessarily imply that the secondary dominates the infrared light, as the amount of secondary star light needed to create an overall red continuum is strongly dependent upon the slope of the secondary star spectrum. The continuum slope in VY Aqr appears to show no variation with orbital phase, always being within one standard error of the mean.

(ii) The water band at $1.33\,\mu\mathrm{m}$ lies in a region affected by telluric features (see Fig. 1), so it is possible that incorrect telluric
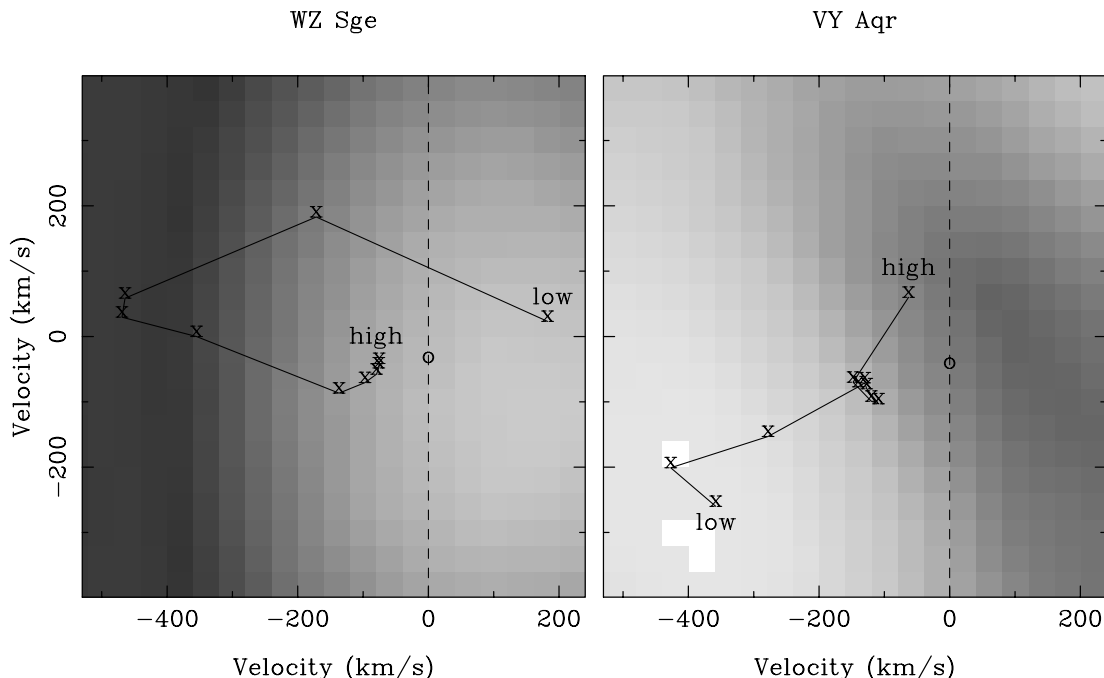

Figure 9. Light centres of the Paschen-β emission in WZ Sge and VY Aqr, superimposed on the Paschen-β Doppler maps. For clarity, strong emission is represented as dark areas for WZ Sge, and light areas for VY Aqr. Points are plotted for double-Gaussian fits with separations ranging from $600\,\mathrm{km\,s}^{-1}$ (marked 'low') to $2400\,\mathrm{km\,s}^{-1}$ (marked 'high'). The dashed line represents $K_X = 0$, and is where the white dwarf is expected to lie. The centre of mass of the white dwarf (marked 'o') is plotted using the values for K_W of Spruit & Rutten (1998) for WZ Sge and Thorstensen & Taylor (1997) for VY Aqr. Phases for WZ Sge are from the ephemeris of Spruit & Rutten; phases for VY Aqr use the ephemeris of Thorstensen & Taylor (1997), with a correction of -0.28 applied.

correction could affect this feature. In order to try and estimate the extent of this effect, spectra of VY Aqr were calibrated using each of the F stars observed. It was seen that there was excess absorption at 1.33 μm, even when the stronger telluric features around 1.14 μm were over-corrected. Therefore incorrect telluric correction cannot account for the observed feature. The presence of the unexplained variations in strength of the water feature with orbital phase (as shown in Fig. 3) is disturbing, however. Following the method outlined above, we find that incorrect telluric correction cannot account for this variation. Also, by repeating the reduction process with a range of parameters and methods, we determine that systematic errors in the reduction process do not account for the variation either. The feature is present in the time-resolved spectra only at a significance of one standard error, so we might attribute the variation in the band to random noise. However, the detection of this feature cannot be regarded as certain. It is noted here that the percentage contributions of the secondary to the *J* band light in VY Aqr and EF Peg are dependent on this feature, and are hence also uncertain.

(iii) The skew-mapping technique correlates with a secondary star template. Strong cross-correlations are obtained with this method. When the time-resolved spectra are averaged in the rest frame of the secondary star, absorption features are stronger and sharper. Further, the skew mapping suggests a correction to the ephemeris for VY Aqr, which is consistent with the radial velocity curves and light curves. Thus we are confident that the skew mapping is correlating with real secondary star features.

None of these items, considered alone, provides concrete signs of the secondary star. However, in combination they provide a strong body of evidence. Hence we are confident that the secondary star has been detected in VY Aqr. The detection in EF Peg is based only on the continuum shape and the water feature at 1.33 μm. Hence the detection of the secondary in this case is less reliable than that in VY Aqr.

6 CONCLUSIONS

We draw the following conclusions.

(i) The relative ease of observation in the *J* band, and strong absorption features of late-type dwarfs in this spectral region make *J* band studies highly desirable for CVs with undetected secondary stars.

(ii) The secondary star has been detected in VY Aqr and EF Peg, although the detection was too weak, and insufficient field-dwarf templates were observed, to make an estimate of the spectral type.

(iii) The contribution of the secondary star to the total *J* band flux was found to be 65 per cent for EF Peg and 70 per cent for VY Aqr. Upper limits of 10 and 20 per cent were found for the contribution of the secondary to the total *J* band flux for WZ Sge and PX And respectively.

(iv) A value of $K_R = 320 \pm 70 \, \text{km s}^{-1}$ was found for VY Aqr, and the mass ratio was calculated as $q = 0.15 \pm 0.04$, assuming that K_W, as derived by Thorstensen & Taylor (1997), is correct.

(v) The spectral type of WZ Sge was constrained to be later than M7.5V.

REFERENCES

Augusteijn T., 1994, A&A, 292, 481
Bessell M. S., 1991, AJ, 101, 662
Ciardi D. R., Howell S. B., Hauschildt P. H., Allard F., 1998, ApJ, 504, 450
Daley P. N., Beard S. M., 1994, Starlink User Note 27, DRAL
Dhillon V. S., 1997, in Howell S. B., ed., Proceedings of the 13th North American Workshop on Cataclysmic Variables and Low Mass X-ray Binaries. SDSU Press, San Diego, p. 23
Dhillon V. S., Marsh T. R., 1995, MNRAS, 275, 89
Friend M. T., Smith R. C., Martin J. S., Jones D. H. P., 1988, MNRAS, 233, 451
Froning C. S., Robinson E. L., Welsh W. F., Wood J. H., 1999, in Hellier C., Mukai K., eds, ASP Conf. Ser. Vol. 157, Annapolis Workshop on Magnetic Cataclysmic Variables. Astron. Soc. Pac., San Francisco, p. 397
Gilliland R. L., Kemper E., Suntzeff N., 1986, ApJ, 301, 252
Henry T. J., Kirkpatrick J. D., Simons D. A., 1994, AJ, 108, 1437
Horne K., 1986, PASP, 98, 609
Howell S. B., Schmidt R., Deyoung J. A., Fried R., Schmeer P., Gritz L., 1993, PASP, 105, 579
Howell S. B., Rappaport S., Politano M., 1997, MNRAS, 287, 929
Jones H. R. A., Longmore A. J., Jameson R. F., Mountain C. M., 1994, MNRAS, 267, 413
Jones H. R. A., Longmore A. J., Allard F., Hauschildt P. H., 1996, MNRAS, 280, 77
Joyce R. R., 1992, in Howell S. B., ed., ASP Conf. Ser. Vol. 23, Astronomical CCD Observing and Reduction Techniques. Astron. Soc. Pac., San Francisco, p. 258
Joyce R. R., Hinkle H. H., Wallace L., Dulick M., Lambert D. L., 1998, AJ, 116, 2520
Kirkpatrick J. D., Kelly D. M., Rieke G. H., Liebert J., Allard F., Wehrse R., 1993, ApJ, 402, 643
Kleinmann S. G., Hall D. N. B., 1986, ApJS, 62, 501
Kolb U., 1993, A&A, 271, 149
Lang K. R., 1986, Astrophysical Formulae. Springer-Verlag, Berlin
Marsh T. R., 1988, MNRAS, 231, 1117
Marsh T. R., 1990, ApJ, 357, 621
Marsh T. R., Horne K., 1988, MNRAS, 235, 269
Patterson J., Bond H. E., Grauer A. D., Shafter A. W., Mattei J. A., 1993, PASP, 105, 69
Ramsay S. K., Mountain C. M., Geballe T. R., 1992, MNRAS, 259, 751
Schneider D. P., Young P. J., 1980, ApJ, 238, 946
Shafter A. W., Szkody P., Thorstensen J. R., 1986, ApJ, 308, 765
Smak J., 1993, Acta Astron., 43, 101
Smith D. A., Dhillon V. S., 1998, MNRAS, 301, 767
Smith D. A., Dhillon V. S., Marsh T. R., 1998, MNRAS, 296, 465
Smith R. C., Cameron A., Tucknott D. S., 1993, in Regev O., Shaviv G., eds, Cataclysmic Variables and Related Physics. Inst. Phys. Publ., Bristol, p. 70
Sproats L. N., Howell S. B., Mason K. O., 1996, MNRAS, 282, 1211

Spruit H. C., Rutten R. G. M., 1998, MNRAS, 299, 768

Still M. D., Dhillon V. S., Jones D. H. P., 1995, MNRAS, 273, 863

Thorstensen J. R., Taylor C. J., 1997, PASP, 109, 1359

Tinney C. G., Mould J. R., Reid I. N., 1993, AJ, 105, 1045

Wade R. A., Horne K., 1988, ApJ, 324, 411

Warner B., 1995, Cataclysmic Variable Stars. Cambridge Univ. Press, Cambridge

Whitehurst R., 1988, MNRAS, 232, 35

This paper has been typeset from a TEX/LATEX file prepared by the author.